

Published in final edited form as:

Nat Plants. 2017 September ; 3(9): 749–754. doi:10.1038/s41477-017-0003-y.

***DELLA* genes restrict inflorescence meristem function independently of plant height**

Antonio Serrano-Mislata^{1,3}, Stefano Bencivenga², Max Bush¹, Katharina Schiessl¹, Scott Boden², and Robert Sablowski^{1,*}

¹Cell and Developmental Biology Department, John Innes Centre, Norwich Research Park, Norwich, NR4 7UH, United Kingdom

²Crop Genetics Department, John Innes Centre, Norwich Research Park, Norwich, NR4 7UH, United Kingdom

Summary

DELLA proteins associate with transcription factors to control plant growth in response to gibberellin 1. Semi-dwarf *DELLA* mutants with improved harvest index and decreased lodging greatly improved global food security during the “green revolution” in the 1960-70s 2. However, *DELLA* mutants are pleiotropic and the developmental basis for their effects on plant architecture remains poorly understood. Here, we show that *DELLA* proteins have genetically separable roles in controlling stem growth and the size of the inflorescence meristem, where flowers initiate. Quantitative 3D image analysis, combined with a genome-wide screen for *DELLA*-bound loci in the inflorescence tip, revealed that *DELLA*s limit meristem size in Arabidopsis by directly up-regulating the cell cycle inhibitor *KRP2* in the underlying rib meristem, without affecting the canonical *WUSCHEL-CLAVATA* meristem size regulators³. Mutation of *KRP2* in a *DELLA* semi-dwarf background restored meristem size, but not stem growth, and accelerated flower production. In barley, secondary mutations in the *DELLA* gain of function mutant *Sln1d4* also uncoupled meristem and inflorescence size from plant height. Our work reveals an unexpected and conserved role for *DELLA* genes in controlling shoot meristem function and suggests how dissection of pleiotropic *DELLA* functions could unlock further yield gains in semi-dwarf mutants.

Growth of the stem and of lateral organs, including leaves and flowers, is initiated at the shoot apical meristem (SAM), where a pool of stem cells continuously provides cells to form new tissues³. During reproductive development, the outer cell layers of the SAM

Users may view, print, copy, and download text and data-mine the content in such documents, for the purposes of academic research, subject always to the full Conditions of use:http://www.nature.com/authors/editorial_policies/license.html#terms

*Correspondence to: robert.sablowski@jic.ac.uk.

³Current address: Instituto de Biología Molecular y Celular de Plantas, Consejo Superior de Investigaciones Científicas-Universidad Politécnica de Valencia, 46022 Valencia, Spain

Author contributions

Conceptualisation, A.S.-M., S.Bo. and R.S.; investigation, A.S.-M., S.Be., M.B., S.Bo. and K.S.; software, R.S.; formal analysis and data curation: A.S.-M. and R.S.; writing – original draft, A.S.-M. and R.S.; writing – review & editing, A. S.-M., S.Be., M.B., S.Bo., K.S. and R.S.; funding acquisition, R.S and A. S.-M.; supervision, R.S.

Competing interests

The authors declare no competing financial interests.

(tunica) give rise to floral buds and contribute cells to form the outer tissues of the stem, whereas the inner stem tissues originate from the subapical region of the SAM, called the rib zone (RZ).

Stem growth is promoted by gibberellin, which binds to the GID1 receptor to promote ubiquitin-dependent degradation of DELLA proteins. Mutations that reduce GA levels or disrupt the interaction between DELLAs and GID1 stabilise DELLAs and consequently inhibit stem growth¹. Arabidopsis has five *DELLA* genes with overlapping functions, of which two (*GA-INSENSITIVE*, *GAI*, and *REPRESSOR of gal-3*, *RGA*) have a predominant role in regulating stem growth⁵ and are transcribed in the inflorescence apex, including the SAM (Supplementary Fig. S1). In accordance with their role in controlling cell proliferation⁶, localised activation of a GA-resistant version of the *GAI* protein⁷ using a Cre-*loxP* recombination system confirmed that most of the inhibitory effect on growth occurred within the apical 2 mm of the inflorescence stem (Supplementary Fig. S1), where cell division is most active⁶.

To understand in detail how *GAI* and *RGA* control stem growth, we looked for the earliest visible defects in the dwarf gain-of-function *gai* mutant and in dwarf transgenic plants expressing a GA-resistant version of *RGA* (*RGAp:GFP-rga 17*)⁸. The *CYCB1;1p:GFP9* reporter showed fewer mitoses in the developing internodes of *gai*, without obvious differences in cell size and before any visible change in internode length (Supplementary Fig. S2), in line with the role of DELLAs in regulating the supply of new cells for internode growth. In addition, *gai* and *RGAp:GFP-rga 17* appeared to reduce SAM size, including the tunica layers and the RZ (Supplementary Fig. S2). Measurements of projected meristem area confirmed that the SAM was smaller not only in *gai* and *RGAp:GFP-rga 17*, but also in the GA-deficient *ga4-1* mutant¹⁰; conversely, *global della* plants, with loss of function of all five Arabidopsis *DELLA* genes¹¹, had a notably enlarged SAM (Fig. 1a-c). The negative role of *DELLA* genes in the inflorescence meristem was unexpected, because gibberellin has been shown to antagonise shoot meristem activity in seedlings¹², in contrast to its positive role in the control of root meristem size^{9,13}. The potentially different roles of *DELLA* in the vegetative and reproductive SAM might reflect other changes in SAM function, such as activation of the rib meristem during flowering.

DELLA proteins interact with transcription factors bound to their target genes, which can be detected by chromatin immunoprecipitation (ChIP) using tagged *DELLA*¹⁴. To reveal the molecular basis for *DELLA* control of stem growth and SAM size, we performed ChIP-seq to detect loci bound by *RGAp:GFP-rga 17* in inflorescence apices. As internal controls, we used ten genes previously shown to be *DELLA*-regulated (Supplementary Table S2, Supplementary Fig. S3). Candidate target genes were selected if the region within 3 kb upstream and 1.5 kb downstream of their coding sequences contained ChIP-seq peaks consistently detected in three *RGAp:GFP-rga 17* replicates (FDR < 0.001) but not in the negative controls. From these genes, we selected 2327 high-confidence candidates with a peak enrichment at least as high as the internal control with the lowest enrichment (*LEAFY*) (Supplementary Table S1, Supplementary Fig. S3). In accordance with *DELLA* roles regulating growth in response to hormonal, developmental and environmental responses¹⁵, the set of high-confidence targets included numerous genes involved in responses to

hormones (GA, auxin, brassinosteroid, abscisic acid and cytokinin), floral transition, organ patterning and growth, floral development and cell wall dynamics (Supplementary Table S2). The list was significantly enriched (p -value 1.2×10^{-50} , Fisher's exact test) for genes bound by GFP-RGA in seedlings 14, but the majority of genes was not shared between the two sets, consistent with DELLA function being conditioned by interaction with tissue-specific transcription factors (Fig. 2 a). Accordingly, the *RGAp:GFP-rga 17* ChIP-seq peaks were significantly enriched for motifs bound by DELLA-interacting transcription factors 14, particularly of the bHLH, bZIP, Dof and SPL families (Supplementary Fig. S3).

The set of high-confidence targets revealed few direct links to the cell cycle machinery (Supplementary Table S2), supporting the idea that DELLA control of cell proliferation is mostly indirect 6. However, the list included three different members (*KRP1*, 2 and 4) of the Kip-related (KRP) family of CDK inhibitors, which play important roles in plant tissue growth 16,17. To investigate direct links between DELLAs and cell cycle control, we focused on *KRP2* because of its higher ChIP-seq peak enrichment relative to *KRP1* and *KRP4* (Supplementary Table S1) and because *KRP2*, but not *KRP1* or *KRP4*, was up-regulated in *gai-3* mutant seedlings 13. Binding of GFP-rga 17 to *KRP2* was independently confirmed by ChIP-qPCR (Fig. 2b,c). A functional *KRP2p:KRP2-GFP* fusion (Supplementary Fig. S4) was expressed weakly below the inflorescence and floral meristems and at lateral organ boundaries (Fig. 2d,f), consistent with the repression of growth in boundary regions 18. In *gai* mutants, *KRP2p:KRP2-GFP* was up-regulated in the rib zone, in floral pedicels and in developing internodes (Fig. 2e,g). Thus, repression of cell proliferation in the inflorescence apex by DELLAs correlated with increased expression of the cell-cycle inhibitor *KRP2*.

We next tested the functional relevance of *KRP2* activation by introducing the *knp2-3* loss-of-function allele 19 into genetic backgrounds with enhanced DELLA activity. To detect the effects of *KRP2* in different meristem regions and to confirm size differences using a method that is not sensitive to meristem geometry, we also measured the number of cells in the tunica and RZ regions. *knp2-3* fully suppressed the reduction in SAM area seen in *gai* and restored cell numbers not only in the RZ, but also in the overlying tunica layers (Fig. 3). However, the more severe defect of *RGAp:GFP-rga 17* and *ga4-1* meristems was only partially suppressed by *knp2-3* (Supplementary Fig. S5), suggesting that *RGA* restricts SAM size through additional genes; plausible candidates would be *KRP1* and *KRP4*. A more specialised role for *RGA* in the inflorescence meristem would be in line with its higher expression in the meristem relative to developing buds (Supplementary Fig. S1). Furthermore, the larger meristem of the *global della* mutant compared to *knp2-3* (Figs. 1a,b and 3C) and the binding of GFP-rga 17 to known regulators of meristem size, such as *CLV1* and cytokinin signalling genes (Supplementary Table S1, Supplementary Fig. S3), suggested that DELLA proteins limit SAM size through additional, *KRP2*-independent mechanisms. In contrast to the effect on meristem size, *knp2-3* did not significantly change stem elongation in wild-type or *gai* background (Figs. 3 a,b), so activation of *KRP2* in developing internodes (Fig. 2 g) is not sufficient to explain the inhibition of stem growth by DELLA proteins. In summary, the effect of semi-dwarf DELLA alleles on SAM size is mediated in part by *KRP2* and is genetically separable from their effect on stem growth.

The localised activation of *KRP2* suggested that DELLA proteins function in the rib zone to regulate SAM growth. SAM size is controlled by the homeodomain protein WUSCHEL (WUS), which is expressed in the rib zone and moves to the overlying tunica layers to specify stem cells marked by *CLAVATA3 (CLV3)* expression 20,21. Neither *WUS* nor *CLV3* fulfilled our criteria for high-confidence ChIP-seq targets of GFP-rga 17 (Supplementary Table S1), however, even if these loci are not directly targeted, their function could still be indirectly affected by DELLA proteins. To test this possibility, we compared expression of *WUSp:GFP-WUS* and *CLV3p:GFP* in *gai* and wild-type SAMs. The number of cells expressing either reporter was not significantly different, while the expression level per cell remained the same for *CLV3p:GFP* and was slightly increased in *gai* for *WUSp:GFP-WUS* (Supplementary Fig. S6), indicating that *KRP2* activation in *gai* did not restrict meristem size by interfering with stem cell maintenance. The effect of rib zone-expressed *KRP2* on the overlying tunica layers could result from mechanical constraints on tissue growth, as proposed to explain how DELLA function localised specifically in the endodermis limits growth of the whole root meristem 9, in contrast with the hypothesis that plant organ growth is mechanically controlled by the outermost cell layers 22.

Changes in SAM size can affect the number of floral buds formed 23 and disrupt their arrangement around the meristem (phyllotaxis) 24. *gai*, *RGAp:GFP-rga 17* or *ga4-1* inflorescence meristems did not show obvious phyllotaxis defects, but the larger meristem of the *global della* mutant did (Fig. 1a). Assuming that successive buds develop at the same speed, we estimated the rate of bud initiation by comparing daily the number of flowers that reached maturity in the main inflorescence of wild-type, *kpr2-3*, *gai*, *gai kpr2-3* and *global della* plants. Reflecting the differences in SAM size, the rate of bud production increased in the *global della* mutant and decreased in *gai* in a *KRP2*-dependent way (Fig. 3i). However, increased meristem longevity in *gai* resulted in a final number of flowers comparable to the wild-type (Fig. 3i). Meristem arrest correlates with seed development 25, although the molecular mechanism remains unknown, so the extended meristem activity in *gai* may result from the reduced fertility of DELLA gain-of-function mutants 26,27. We conclude that the *KRP2*-dependent decrease in meristem size in *gai* plants had a negative effect on meristem function, but the effect on final floral numbers depended also on meristem longevity.

To test whether the role of DELLA in SAM size is conserved in diverse angiosperms, we analyzed mutants for the barley DELLA gene, *SLENDER1 (SLNI)* 4. The barley inflorescence (spike) has a main axis (rachis) with nodes that support branches (spikelets), each containing a determined number of flowers (florets). 3D imaging of the inflorescence meristem when spikelets were initiated (double ridge stage) 28 revealed that the SAM had significantly fewer cells in the gain-of-function mutant *Sln1d4*, compared with the corresponding wild-type (Himalaya) ($p = 6.54 \times 10^{-3}$, $n = 7$, Mann-Whitney's test; Fig. 4f). To test whether control of meristem size is also separable from other DELLA functions in barley, we took advantage of an allelic series of *Sln1d4*. The *Sln1d5* and *Sln1d6* alleles, which contain second-site mutations in *Sln1d*, have similar effects on a subset of the DELLA gain-of-function phenotypes, partially restoring leaf elongation 4 and plant height (Fig. 4a). In spite of these similarities, *Sln1d5* and *Sln1d6* differentially affected meristem size (Fig. 4c-f). Furthermore, SAM size correlated with the number of rachis nodes produced by the SAM (Fig. 4b, f). Uncoupling of plant height from SAM size was also shown by the

comparable meristems but distinct height of *Sln1d* and *Sln1d.5* (Fig.4a,f). In conclusion, DELLA-induced restriction of meristem size led to reduced inflorescence size in a cereal crop. The smaller inflorescence of *Sln1d* is reminiscent of the lower number of flowers seen in the rice semi-dwarf mutant *sd1 29*, which like *ga4-1* affects gibberellin biosynthesis, although it is not known whether *sd1* also affects inflorescence meristem size.

Overall, our results show that DELLA genes have a conserved role in limiting inflorescence meristem size, in line with the role of DELLA in saving resources under environmental stress 15. This function involves a direct link to cell cycle regulation in the rib meristem and is genetically separable from the role of DELLAs in subsequent organ growth. Because the size of the inflorescence meristem limits yield potential in crop plants 23,30, separating the effects of DELLA on stem growth and meristem size could unlock further yield increases in the widely-used semi-dwarf mutants.

Methods

Plant material

Arabidopsis thaliana Landsberg *erecta* (L-*er*) accession was used as wild type unless otherwise specified. *gai 31*, *RGAp:GFP-rga 1726*, *ga4-1 10*, *global della 11*, *krp2-3 19* (backcrossed three times to L-*er*), *jag-1 krp2-317*, *CYCB1;1p:GFP9*, *GAIp:GUS 32*, *RGAp:GFP-RGA 33*, *WUSp:GFP-WUS 21*, *CLV3p:GFP 34*, *35Sp:loxGUSlox-GFP 35* and *hsp18.2:Cre 36* have been described. *35SploxGUSloxgaiGFP*, *35Sp:lox-GFP-lox-GUS* and *KRP2p:KRP2-GFP* were constructed and transformed into *Arabidopsis* as described in the Supplementary Information. *Arabidopsis* plants were grown on JIC *Arabidopsis* Soil Mix (Levington F2 compost with Intercept and 4-mm grit at a 6:1 ratio) at 16°C under continuous light. Dissection of inflorescence apices for imaging, ChIP, and measurement of plant height were performed when the plants had produced the first three mature flowers. The Barley (*Hordeum vulgare*) Himalaya (wild-type), *Sln1d* (M640), *Sln1d.5* (TR9) and *Sln1d.6* (TR13) mutants 4 were grown on JIC Cereal Mix (containing 1.3kg/m³ PG Mix 14-16-18 and 1kg/m³ Osmocote Mini 16-8-11 2 mg) under long day photoperiod (16 h light/8 h dark) and 20°C/15°C day/night temperatures. Barley inflorescence apices were dissected for imaging at the double ridge stage 37.

Cre-loxP recombination

hsp18.2:Cre, *35Sp:lox-GUS-lox-gai-GFP* and *hsp18.2:Cre*, *35Sp:lox-GUS-lox-GFP* plants were grown until they had three self-pollinated flowers. Open flowers were removed and ink marks were placed on the stem. For localised heat-shock, water at 38.5 °C was streamed for 5 minutes onto a 2 mm sponge clamped around the stem. Plants were photographed after 10 days of growth and distances between ink marks were measured with Fiji 38. Similarly treated *hsp18.2:Cre*, *35Sp:lox-GFP-lox-GUS* were stained for GUS 36 30 h after heat shock.

Growth measurements

Arabidopsis stem height was measured from photographs using Fiji 38. To determine the rate of floral initiation, plants were grown at 16 °C under continuous light; starting on the day floral buds became visible, flowers at stage 13 and beyond 39 were counted daily in the

main inflorescence of 8 to 10 plants per genotype. The whole experiment was repeated three times with similar results. Rachis nodes in barley inflorescences were counted for the main stem and first tiller in two independent experiments.

Confocal imaging

Dissection, of shoot apices, live imaging and modified pseudo-Schiff propidium iodide (mPS-PI) staining were as described 40,41, before imaging with a Zeiss LSM780 confocal microscope; resolution was 0.42 x 0.42 x 0.50 μm for Arabidopsis and 0.66 x 0.66 x 1.0 μm for barley. GFP was imaged in cleared apices by the ClearSee method 42 before imaging with a Leica SP5 confocal microscope with a 20x/0.75 long-working distance objective (resolution 0.63 x 0.63 x 1 μm). Vibratome sectioning is described in the Supplementary Information.

Image analysis

Custom Python scripts and Fiji macros based on a previous set of scripts 40,41 were used to segment confocal image stacks, measure shoot meristem areas, define the position of cells within the shoot meristem and measure GFP signal within segmented cells. The function of each script is summarised in the Supplementary Information. Supplementary Table S3 lists the scripts used to produce the data for each manuscript figure and Supplementary Table S4 lists the filtering parameters (e.g. to select cells in meristem regions). The annotated source code with detailed instructions and folders containing the confocal images, files produced during image processing and final cell data tables are publicly available (see Data Availability).

Statistics

Data were read and processed in a Python shell using the functions defined and annotated in script /3D_meristem_analysis/python_scripts/statistical_analysis.py (within Supplemental Software, DOI: [10.6084/m9.figshare.4675801](https://doi.org/10.6084/m9.figshare.4675801)), using Scientific Python (<http://www.scipy.org>) functions for linear regression, Shapiro-Wilk tests for normality, two-tailed Student's *t*-tests and two-tailed Mann-Whitney tests. For samples with *n* less than 100, power analysis was performed with the *pwr* package in R (<http://www.r-project.org/>), using function *pwr.t2n.test* to calculate effect sizes, assuming a significance level of 0.05, power 0.8, and the alternative hypothesis that the mean was smaller for sample 2 than for sample 1. Raw values, descriptive statistics, *p*-values and effect sizes for the data used in each figure are listed in Supplementary Table S4. In all figures with boxplots, boxes extend from the lower to the upper quartile, with a line marking the median, and whiskers extend to 1.5 times the interquartile range.

ChIP-seq and data analysis

Dissected inflorescence apices of *RGAp:GFP-rga 17* and *L-er* (wt) plants were collected at the same stage used for imaging. Developing siliques and open flowers were removed and the remaining apex was dissected, including 2-5 mm of stem below the SAM. Because DELLA proteins are thought to bind DNA indirectly through interactions with transcription factors, the tissue was fixed with 2% formaldehyde in PBS 1x supplemented with 1 μM

Di(N-succinimidyl) glutarate (DSG; Synchem) under vacuum for 20 min to improve protein-protein and protein-DNA crosslinks. Crosslinking was stopped with 100 μ M glycine and after two washes with water, the samples were blotted dry and frozen in liquid nitrogen. The subsequent ChIP, generation of ChIP-seq libraries and analysis were performed as described 40. To detect enriched sequence motifs, MEME-ChIP was used in discriminative mode (<http://meme-suite.org/tools/meme-chip>)⁴³, comparing peak sequences with a ten-fold larger control set of random peaks as described 40. Raw and processed ChIP-seq data have been deposited at NCBI's Gene Expression Omnibus 44 (see Data Availability).

ChIP-PCR

ChIP-qPCR was performed on *RGAp:GFP-rga 17* and *L-er* (wt) dissected inflorescence apices as described 17, using the 2^{-Ct} method 45 to calculate the relative abundance of immunoprecipitated DNA, compared with controls containing a constant amount of input DNA. The following primers were used for each amplicon: KRP2 -1.6 5'-TGATTGAGTATGCAGCTCGTG-3' and 5'-AATGCCGTCGTTCTGTATCG-3'; KRP2 +1.3 5'-CCCACGAGGCAAAGATTTTA-3' and 5'-GTGGAGAAAAGACTCCAGCTC-3'; *MU-like* 5'-GATTTACAAGGAATCTGTTGGTGGT-3' and 5'-CATAACATAGTTTAGAGCATCTGC-3'; FBL17: 5'-AAGTACAGTGGATCCCAACGTC-3' and 5'-GCTAATTGAAAGAGCGTGAGGTC-3'.

Data availability

Source data for all boxplots are listed in Supplementary Table 4; original ChIP-PCR data are found in Supplementary Table S5. Raw and processed ChIP-seq data have been deposited at NCBI's Gene Expression Omnibus, (<https://www.ncbi.nlm.nih.gov/geo/query/acc.cgi?acc=GSE94926>, accession GSE94926). The source code for image analysis and detailed instructions are available as Supplementary software (DOI: [10.6084/m9.figshare.4675801](https://doi.org/10.6084/m9.figshare.4675801)). For each image folder listed on Supplementary Tables S3 and S4, the original confocal images, processed images, associated cell data and metadata files data can be downloaded at <https://figshare.com> (DOI: [10.6084/m9.figshare.4675801](https://doi.org/10.6084/m9.figshare.4675801)).

Supplementary Material

Refer to Web version on PubMed Central for supplementary material.

Acknowledgments

We thank Peter Chandler, Lars Østergaard, Tai-Ping Sun, Nick Harberd, Peter Doerner, Venugopala Reddy, Miguel Ángel Pérez Amador and the European Arabidopsis Stock Centre for plasmids and seeds, Grant Calder for advice with confocal microscopy and Bihai Shi for help with vibratome sections. The work was supported by BBSRC grants BB/J007056/1, BB/J004588/1 and BB/M003825/1, and by a grant from the Ministerio de Educación, Cultura y Deporte, Spain (EX-2010-0491) to ASM.

References

1. Daviere J-M, Achard P. Gibberellin signaling in plants. *Development*. 2013; 140:1147–1151. DOI: 10.1242/dev.087650 [PubMed: 23444347]

2. Pingali PL. Green revolution: impacts, limits, and the path ahead. *Proc Natl Acad Sci U S A*. 2012; 109:12302–12308. DOI: 10.1073/pnas.0912953109 [PubMed: 22826253]
3. Holt AL, van Haperen JM, Groot EP, Laux T. Signaling in shoot and flower meristems of *Arabidopsis thaliana*. *Curr Opin Plant Biol*. 2014; 17:96–102. [PubMed: 24507500]
4. Chandler PM, Harding CA. ‘Overgrowth’ mutants in barley and wheat: new alleles and phenotypes of the ‘Green Revolution’ *Della* gene. *J Exp Bot*. 2013; 64:1603–1613. [PubMed: 23382550]
5. King KE, Moritz T, Harberd NP. Gibberellins are not required for normal stem growth in *Arabidopsis thaliana* in the absence of *GAI* and *RGA*. *Genetics*. 2001; 159:767–776. [PubMed: 11606551]
6. Daviere JM, et al. Class I TCP-DELLA interactions in inflorescence shoot apex determine plant height. *Curr Biol*. 2014; 24:1923–1928. DOI: 10.1016/j.cub.2014.07.012 [PubMed: 25127215]
7. Peng J, et al. The *Arabidopsis* *GAI* gene defines a signaling pathway that negatively regulates gibberellin responses. *Genes Dev*. 1997; 11:3194–3205. [PubMed: 9389651]
8. Dill A, Sun TP. Synergistic derepression of gibberellin signaling by removing *RGA* and *GAI* function in *Arabidopsis thaliana*. *Genetics*. 2001; 159:777–785. [PubMed: 11606552]
9. Ubeda-Tomas S, et al. Gibberellin signaling in the endodermis controls *Arabidopsis* root meristem size. *Curr Biol*. 2009; 19:1194–1199. [PubMed: 19576770]
10. Koornneef M, van der Veen JH. Induction and analysis of gibberellin sensitive mutants in *Arabidopsis thaliana* (L.) heynh. *Theor Appl Genet*. 1980; 58:257–263. DOI: 10.1007/BF00265176 [PubMed: 24301503]
11. Koini MA, et al. High Temperature-Mediated Adaptations in Plant Architecture Require the bHLH Transcription Factor *PIF4*. *Curr Biol*. 2009; 19:408–413. DOI: 10.1016/j.cub.2009.01.046 [PubMed: 19249207]
12. Jasinski S, et al. *KNOX* action in *Arabidopsis* is mediated by coordinate regulation of cytokinin and gibberellin activities. *Curr Biol*. 2005; 15:1560–1565. [PubMed: 16139211]
13. Achard P, et al. Gibberellin signaling controls cell proliferation rate in *Arabidopsis*. *Curr Biol*. 2009; 19:1188–1193. DOI: 10.1016/j.cub.2009.05.059 [PubMed: 19576768]
14. Marín-de la Rosa N, et al. Genome Wide Binding Site Analysis Reveals Transcriptional Coactivation of Cytokinin-Responsive Genes by *DELLA* Proteins. *PLoS Genet*. 2015; 11:e1005337. [PubMed: 26134422]
15. Achard P, et al. Integration of plant responses to environmentally activated phytohormonal signals. *Science*. 2006; 311:91–94. [PubMed: 16400150]
16. De Veylder L, et al. Functional analysis of cyclin-dependent kinase inhibitors of *Arabidopsis*. *The Plant Cell*. 2001; 13:1653–1668. [PubMed: 11449057]
17. Schiessl K, Muino JM, Sablowski R. *Arabidopsis* *JAGGED* links floral organ patterning to tissue growth by repressing Kip-related cell cycle inhibitors. *Proceedings of the National Academy of Sciences of the United States of America*. 2014; 111:2830–2835. DOI: 10.1073/pnas.1320457111 [PubMed: 24497510]
18. Rast MI, Simon R. The meristem-to-organ boundary: more than an extremity of anything. *Curr Opin Genet Dev*. 2008; 18:287–294. [PubMed: 18590819]
19. Sanz L, et al. The *Arabidopsis* D-type cyclin *CYCD2;1* and the inhibitor *ICK2/KRP2* modulate auxin-induced lateral root formation. *Plant Cell*. 2011; 23:641–660. DOI: 10.1105/tpc.110.080002 [PubMed: 21357490]
20. Mayer KF, et al. Role of *WUSCHEL* in regulating stem cell fate in the *Arabidopsis* shoot meristem. *Cell*. 1998; 95:805–815. [PubMed: 9865698]
21. Yadav RK, et al. *WUSCHEL* protein movement mediates stem cell homeostasis in the *Arabidopsis* shoot apex. *Genes Dev*. 2011; 25:2025–2030. [PubMed: 21979915]
22. Savaldi-Goldstein S, Peto C, Chory J. The epidermis both drives and restricts plant shoot growth. *Nature*. 2007; 446:199. [PubMed: 17344852]
23. Je BI, et al. Signaling from maize organ primordia via *FASCIATED EAR3* regulates stem cell proliferation and yield traits. *Nat Genet*. 2016; 48:785–791. DOI: 10.1038/ng.3567 [PubMed: 27182966]

24. Leyser HO, Furner I. Characterisation of three shoot apical meristem mutants of *Arabidopsis thaliana*. *Development*. 1992; 116:397–403.
25. Hensel LL, Nelson MA, Richmond TA, Bleecker AB. The fate of inflorescence meristems is controlled by developing fruits in *Arabidopsis*. *Plant Physiol*. 1994; 106:863–876. [PubMed: 7824655]
26. Dill A, Jung HS, Sun TP. The DELLA motif is essential for gibberellin-induced degradation of RGA. *Proceedings of the National Academy of Sciences of the United States of America*. 2001; 98:14162–14167. [PubMed: 11717468]
27. Huang S, et al. Transgenic studies on the involvement of cytokinin and gibberellin in male development. *Plant Physiol*. 2003; 131:1270–1282. DOI: 10.1104/pp.102.018598 [PubMed: 12644677]
28. Waddington SR, Cartwright PM, Wall PC. A Quantitative Scale of Spike Initial and Pistil Development in Barley and Wheat. *Ann Bot*. 1983; 51:119–130.
29. Ashikari M, et al. Cytokinin oxidase regulates rice grain production. *Science*. 2005; 309:741–745. [PubMed: 15976269]
30. Xu C, et al. A cascade of arabinosyltransferases controls shoot meristem size in tomato. *Nat Genet*. 2015; 47:784–792. [PubMed: 26005869]
31. Koorneef M, et al. A Gibberellin Insensitive Mutant of *Arabidopsis thaliana*. *Physiol Plant*. 1985; 65:33–39. DOI: 10.1111/j.1399-3054.1985.tb02355.x
32. Gallego-Giraldo C, et al. Role of the gibberellin receptors *GID1* during fruit-set in *Arabidopsis*. *Plant J*. 2014; 79:1020–1032. DOI: 10.1111/tj.12603 [PubMed: 24961590]
33. Silverstone AL, et al. Repressing a repressor: Gibberellin-induced rapid reduction of the RGA protein in *Arabidopsis*. *Plant Cell*. 2001; 13:1555–1565. [PubMed: 11449051]
34. Reddy GV, Meyerowitz EM. Stem-cell homeostasis and growth dynamics can be uncoupled in the *Arabidopsis* shoot apex. *Science*. 2005; 310:663–667. [PubMed: 16210497]
35. Gallois JL, Woodward C, Reddy GV, Sablowski R. Combined SHOOT MERISTEMLESS and WUSCHEL trigger ectopic organogenesis in *Arabidopsis*. *Development*. 2002; 129:3207–3217. Unsp dev0423. [PubMed: 12070095]
36. Sieburth LE, Drews GN, Meyerowitz EM. Non-autonomy of *AGAMOUS* function in flower development: use of a Cre/loxP method for mosaic analysis in *Arabidopsis*. *Development*. 1998; 125:4303–4312. [PubMed: 9753684]
37. Waddington S, Cartwright P, Wall P. A quantitative scale of spike initial and pistil development in barley and wheat. *Ann Bot*. 1983; 51:119–130.
38. Schindelin J, et al. Fiji: an open-source platform for biological-image analysis. *Nat Methods*. 2012; 9:676–682. [PubMed: 22743772]
39. Smyth DR, Bowman JL, Meyerowitz EM. Early flower development in *Arabidopsis*. *Plant Cell*. 1990; 2:755–767. DOI: 10.1105/tpc.2.8.755 [PubMed: 2152125]
40. Bencivenga S, Serrano-Mislata A, Bush M, Fox S, Sablowski R. Control of Oriented Tissue Growth through Repression of Organ Boundary Genes Promotes Stem Morphogenesis. *Dev Cell*. 2016; 39:198–208. DOI: 10.1016/j.devcel.2016.08.013 [PubMed: 27666746]
41. Serrano-Mislata A, Schiessl K, Sablowski R. Active control of cell size generates spatial detail during plant organogenesis. *Curr Biol*. 2015; 25:2991–2996. DOI: 10.1016/j.cub.2015.10.008 [PubMed: 26526374]
42. Kurihara D, Mizuta Y, Sato Y, Higashiyama T. ClearSee: a rapid optical clearing reagent for whole-plant fluorescence imaging. *Development*. 2015; 142:4168–4179. [PubMed: 26493404]
43. Bailey TL, et al. MEME Suite: tools for motif discovery and searching. *Nucleic Acids Res*. 2009; 37:W202.doi: 10.1093/nar/gkp335 [PubMed: 19458158]
44. Edgar R, Domrachev M, Lash AE. Gene Expression Omnibus: NCBI gene expression and hybridization array data repository. *Nucleic Acids Res*. 2002; 30:207–210. [PubMed: 11752295]
45. Livak KJ, Schmittgen TD. Analysis of relative gene expression data using real-time quantitative PCR and the 2(T)(-Delta Delta C) method. *Methods*. 2001; 25:402–408. DOI: 10.1006/meth.2001.1262 [PubMed: 11846609]

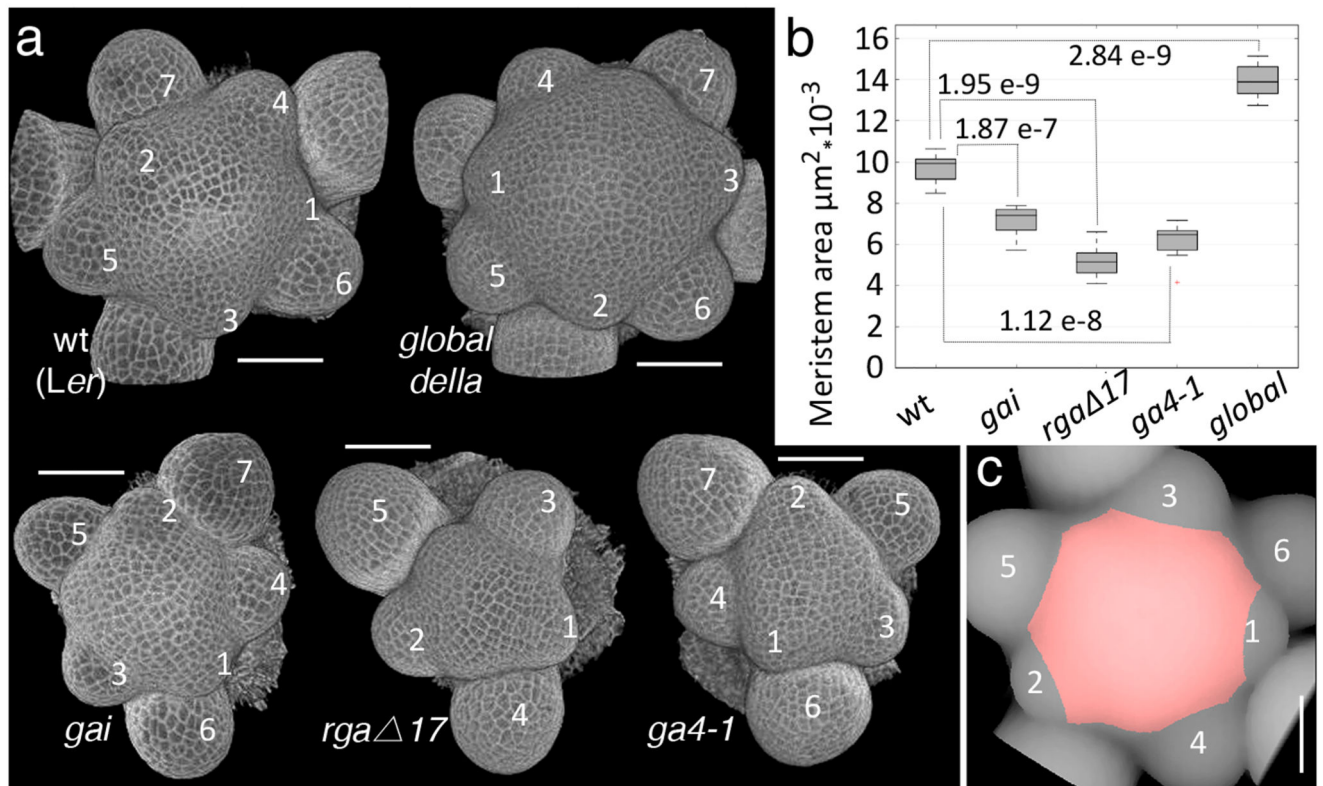


Fig. 1. DELLA proteins control inflorescence meristem size.

(a) 3D reconstructions from confocal stacks of shoot apices stained by the modified pseudo-Schiff propidium iodide (mPS-PI) method; *rga 17* is short for *RGAp:GFP-rga 17* and *global della* is the quintuple mutant *gai-t6, rga-t2, rgl1-1, rgl2-1, and rgl3-411*; numbers indicate floral buds emerging from the SAM, in order of age (youngest marked 1). (b) Boxplots showing projected SAM area in genetic backgrounds with altered DELLA function (10 apices each for wt, *gai* and *ga4-1*; 8 each for *rga 17* and *global della*); *p*-values are for equality of means (Student's *t*-test). (c) Illustration of how projected SAM areas were measured; in this vertical projection of a wt inflorescence apex, the measured region in red corresponds to the meristem surface determined on a 3D image using landmarks placed on bud boundaries (details in Materials and Methods). Bars: 50 μm .

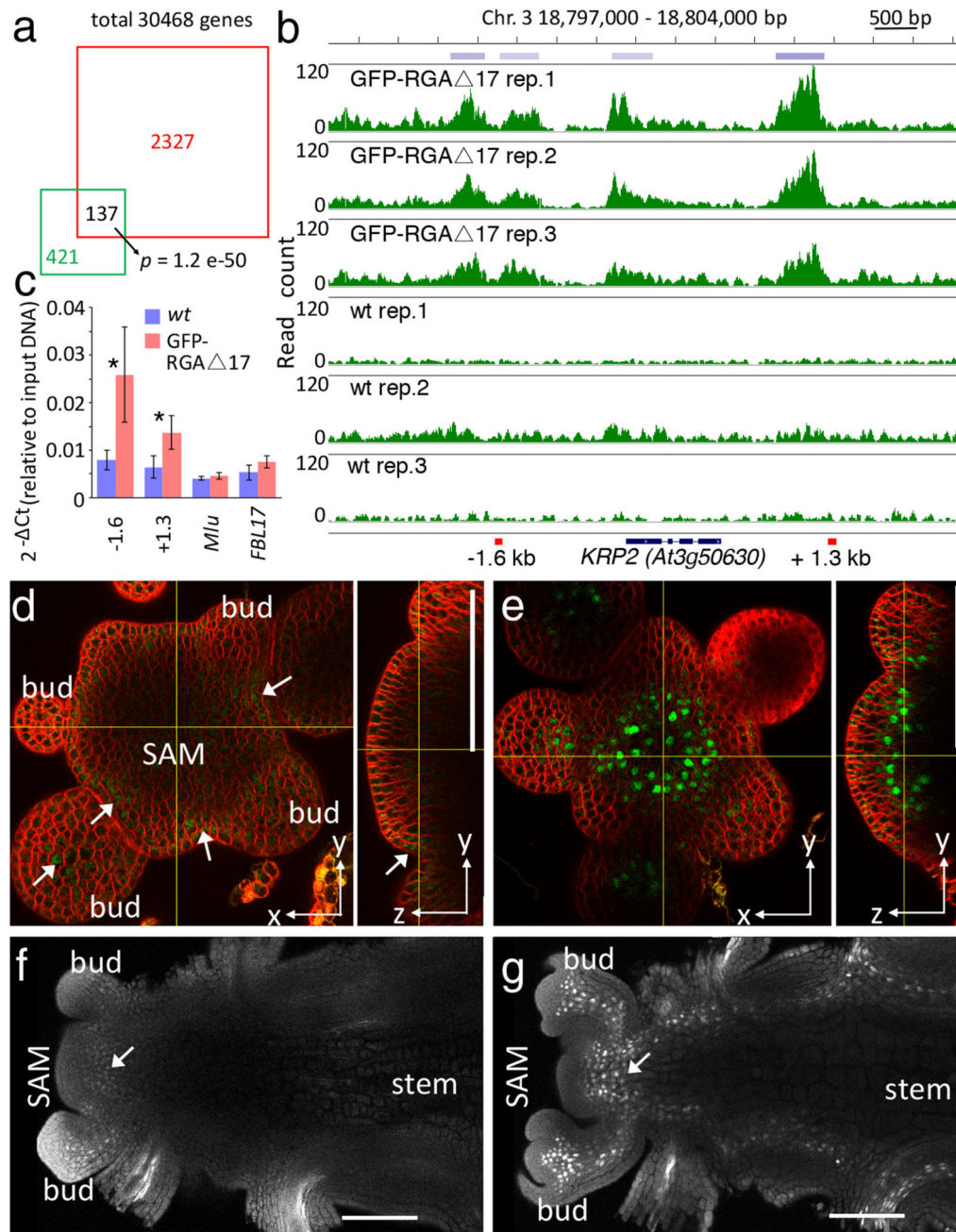


Fig. 2. The cell-cycle inhibitor *KRP2* is a direct DELLA target in the shoot apex.

(a) Overlap between RGA target genes identified by ChIP-seq in inflorescence apices (red square) and seedlings 14 (green square); the p -value is for the overlap occurring by chance (Fisher's exact test, considering a universe of 30,468 genes). (b) Read frequency histograms showing binding of GFP-rga 17 to *KRP2* in triplicate ChIP-seq experiments and wild-type controls; top: chromosome position and regions detected as reproducible peaks (blue bars); bottom: black bars and lines indicate *KRP2* exons and introns, respectively, and red bars show the regions amplified in the ChIP-qPCR experiment. (c) ChIP-qPCR confirming

binding of GFP-*rga 17* protein to *KRP2*; -1.6 kb and +1.3 kb indicate the position of amplified regions relative to the *KRP2* coding sequence; negative controls were *MU-like* transposon (*Mlu*) and the promoter region of the *F-BOX-LIKE 17* gene (*FBL17*, a representative locus not bound by GFP-*rga 17* in the ChIP experiment; Supplementary Fig. S3); bars and lines show means and standard deviation of three biological replicates and asterisks indicate significant difference to the wild type ($p < 0.05$, Student t-test; source data in Supplementary Table S5). (d-g) Confocal images showing *KRP2p:KRP2-GFP* expression in wild-type (arrows in d, f) and *gai* (e, g) inflorescence apices, shown as orthogonal views of the inflorescence meristem stained with FM4-64 (d,e) and longitudinal sections of cleared apices (f, g).

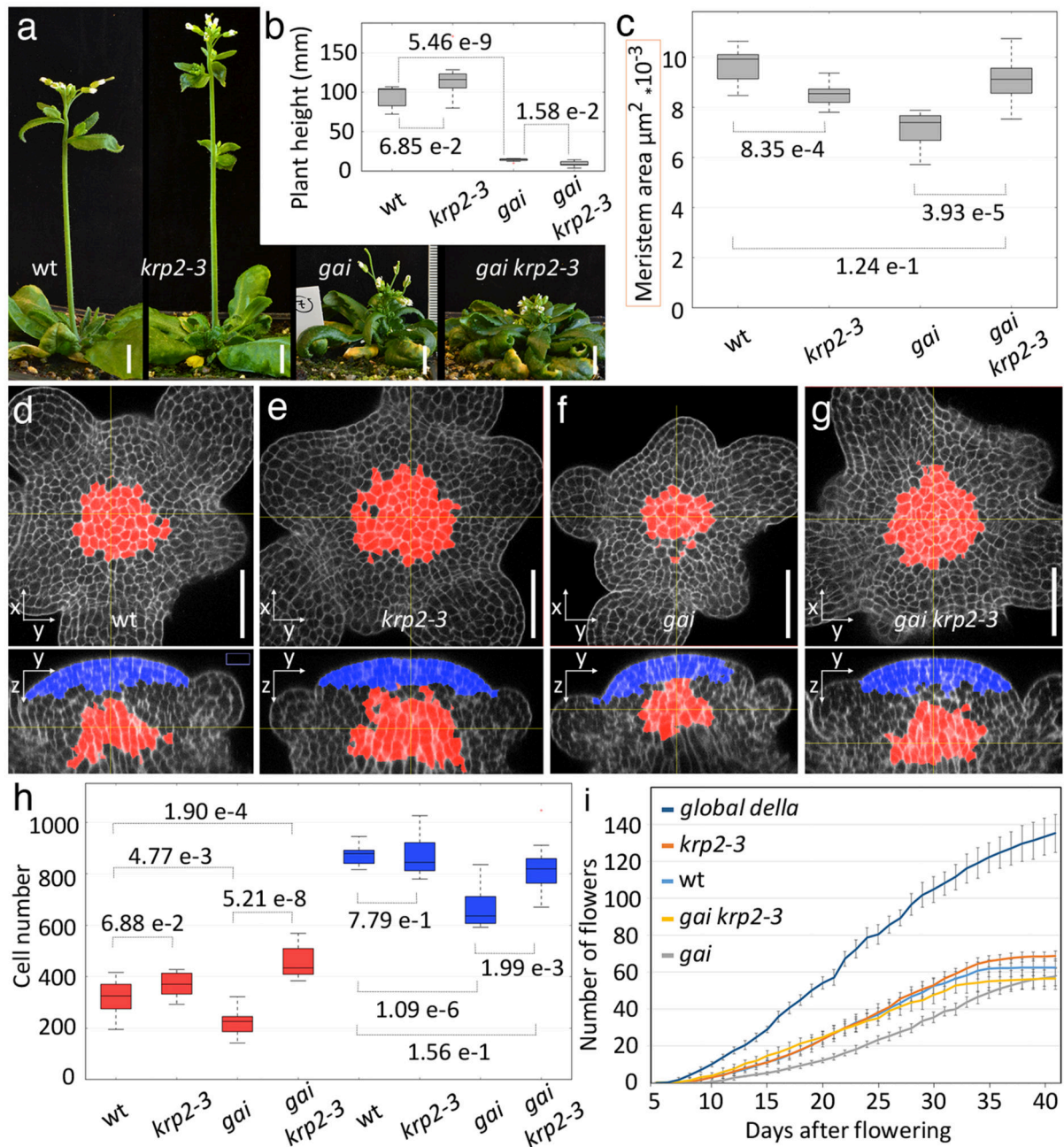


Fig. 3. KRP2 mediates DELLA control of meristem size and bud production but not stem elongation.

(a) Representative images of *L-er* (wild-type), *krp2-3*, *gai* and *gai krp2-3* plants with 3-5 mature flowers. (b) Boxplots of plant height at the stage shown in (a) (7 plants per genotype). (c) Boxplot of SAM areas measured as in Fig. 1 for wild type, *krp2-3*, *gai* and *gai krp2-3* (10, 8, 10 and 10 plants, respectively). (d-g) Orthogonal views of confocal image stacks of representative inflorescence apices stained with mPs-PI; within the meristem, defined using landmarks placed on bud boundaries, the RZ (red) was selected as a region within 90 μm of a plane crossing the meristem summit and normal to the main SAM axis,

with consistently thicker walls (based on mPS-PI signal) and vertically oriented divisions (based on the orientation of the thinnest wall); the tunica region (blue) was selected within 15 μm of the meristem surface and 30 μm from the plane crossing the summit (details in Supplementary Information). (h) Boxplots of cell numbers in the tunica (blue) and RZ (red) regions for different genotypes (11 plants for *krip2-3*, 10 for other genotypes). (i) Cumulative number of mature flowers in the main inflorescence of wild-type, *krip2-3*, *gai*, *gai krip2-3* and *global della* plants (average and SD for 10 plants per genotype); day 0 was when floral buds were first visible by eye. Bars: 1 cm (a), 50 μm (d-g); *p*-values in b, c, h are for equality of means (Student's *t*-test).

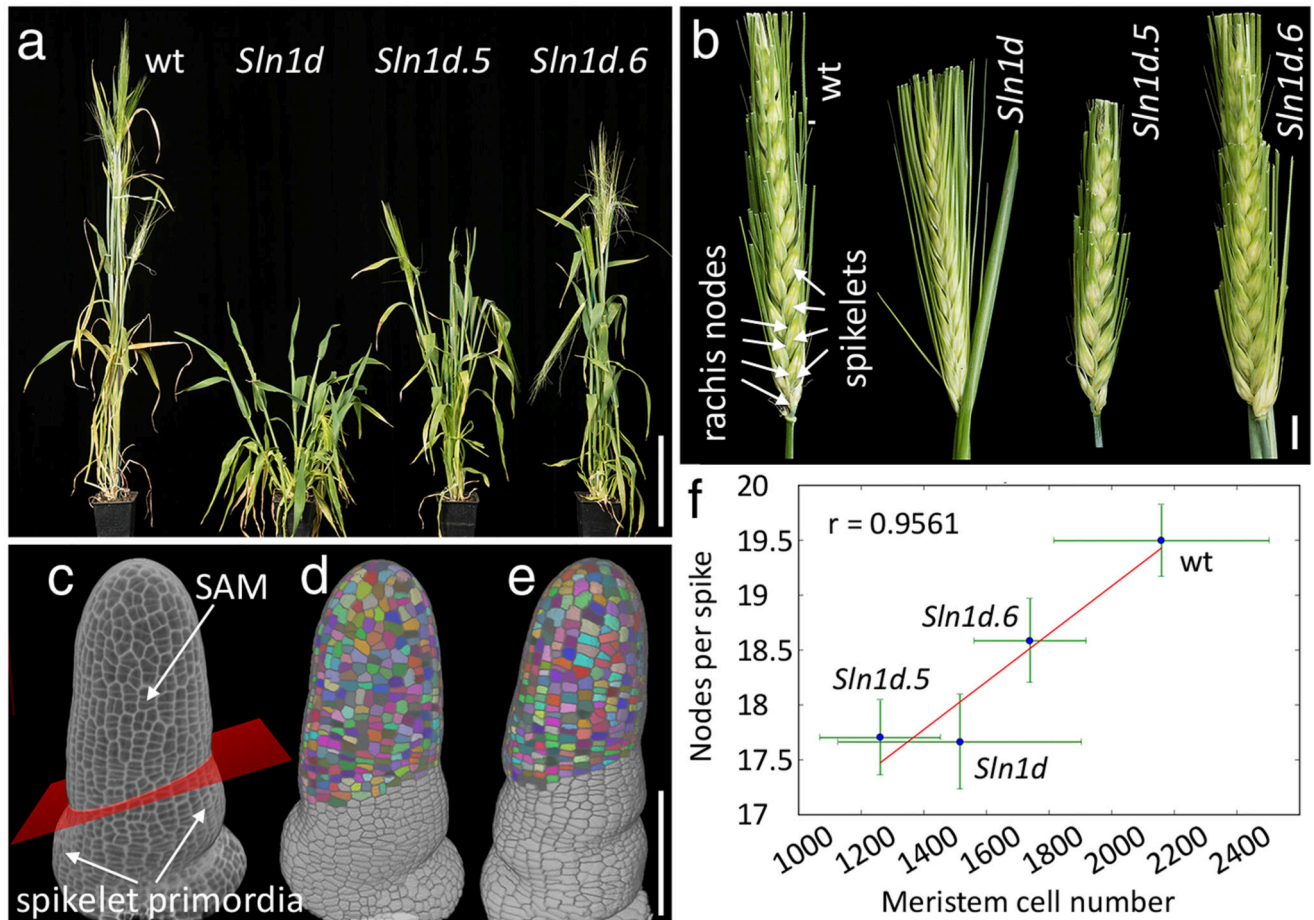


Fig. 4. DELLA control of meristem size is conserved and correlates with inflorescence size in barley.

(a) Wild type barley (Himalaya) and *della* mutants (*Sln1d*, *Sln1d5*, *Sln1d6*) at comparable stages after flowering. (b) Mature spikes of genotypes shown in (a), with alternating spikelets attached to nodes of the main axis (rachis) indicated for the wild type. (c) 3D reconstruction of confocal image of mPS-PI-stained wild-type inflorescence meristem, fixed when the first spikelet primordia were initiated; a plane (red) fitted to landmarks placed on the boundaries of spikelet primordia was used to select SAM cells (details in Supplementary Information). (d, e) 3D reconstructions of segmented images of wild-type (d) and *Sln1d* (e) apices, with selected SAM cells coloured. (f) Correlation between meristem size (cell numbers) and inflorescence size (rachis nodes) in the wild type and *sln1* mutants; points and green lines show average and standard deviation per genotype, the red line shows the linear regression of averages, with correlation coefficient r ; for Hymalaya, *Sln1d*, *Sln1d5* and *Sln1d6*, respectively, n was 18, 15, 18, 18 spikes (for node numbers) and 8, 7, 3, 4 apices (to image cell numbers). Bars: 10 cm (a), 1 cm (b), 100 μ m (c-e).